Experimental and Ab Initio Dynamical Investigations of the Kinetics and Intramolecular Energy Transfer Mechanisms for the OH + 1,3-Butadiene Reaction between 263 and 423 K at Low Pressure

Deepali Vimal,[†] Alexander B. Pacheco,[‡] Srinivasan S. Iyengar,*[,‡,§] and Philip S. Stevens*[,†,‡]

Center for Research in Environmental Science, School of Public and Environmental Affairs, Department of Chemistry, and Department of Physics, Indiana University, Bloomington, Indiana 47405

Received: January 15, 2008; Revised Manuscript Received: April 21, 2008

The rate constants for the reaction of the OH radical with 1,3-butadiene and its deuterated isotopomer has been measured at 1−6 Torr total pressure over the temperature range of 263−423 K using the discharge flow system coupled with resonance fluorescence/laser-induced fluorescence detection of OH. The measured rate constants for the OH + 1,3-butadiene and OH + 1,3-butadiene-d_6 reactions at room temperature were found to be $(6.98 \pm 0.28) \times 10^{-11}$ and $(6.94 \pm 0.38) \times 10^{-11}$ cm^3 molecule^{-1} s^{-1}, respectively, in good agreement with previous measurements at higher pressures. An Arrhenius expression for this reaction was determined to be $k_1^{II}(T) = (7.23 \pm 1.2) \times 10^{-11}\exp[(664 \pm 49)/T]$ cm^3 molecule^{-1} s^{-1} at 263−423 K. The reaction was found to be independent of pressure between 1 and 6 Torr and over the temperature range of 262− 423 K, in contrast to previous results for the OH + isoprene reaction under similar conditions. To help interpret these results, ab initio molecular dynamics results are presented where the intramolecular energy redistribution is analyzed for the product adducts formed in the OH + isoprene and OH + butadiene reactions.

I. Introduction

1,3-Butadiene is a hazardous, carcinogenic, and genotoxic air pollutant that is extensively used in industry.[1–3] It has predominantly anthropogenic sources such as polymer manufacturing,[4,5] tobacco smoke,[6–8] evaporative emissions from the petroleum industry as well as motor vehicle exhaust,[9–11] in addition to emissions from forest fires and prescribed burning.[12] As a result, the atmospheric fate of 1,3-butadiene is of significant interest due to potential widespread human exposure.

Mixing ratios of 1,3-butadiene in urban air are typically in the range of 0.1−10 ppbv.[4,13] Significantly higher concentrations have been observed inside of moving vehicles,[14] in road traffic tunnels,[15] and near industrial facilities.[12,16] Because of its physicochemical properties, 1,3-butadiene is thought to partition primarily into the atmosphere.[2] Thus, its environmental fate and transformation are determined by its atmospheric reactions.

In the troposphere 1,3-butadiene reacts with OH radicals, NO_3 radicals, O_3, and Cl atoms.[17–20] The reaction of 1,3-butadiene with the hydroxyl radical is considered to be the dominant chemical loss process during the daytime, with lifetimes of 1 and 4.5 h for OH concentrations of approximately 2×10^6 and 8×10^5 molecule cm^{-3}.[20,21] A generic mechanism for the OH-initiated oxidation of 1,3-butadiene is shown below:

$$CH_2{=}CHCH{=}CH_2 + OH \rightarrow (HO)CH_2\bullet CHCH{=}CH_2 \text{ (Adduct)} \quad (1)$$

$$(HO)CH_2\bullet CHCH{=}CH_2 + O_2 \rightarrow (HO)CH_2(OO\bullet)CHCH{=}CH_2 \quad (2)$$

$$(HO)CH_2(OO\bullet)CHCH{=}CH_2 + NO \rightarrow (HO)CH_2(O\bullet)CHCH{=}CH_2 + NO_2 \quad (3a)$$

$$\rightarrow (HO)CH_2(ONO_2\bullet)CHCH{=}CH_2 \quad (3b)$$

$$(HO)CH_2(O\bullet)CHCH{=}CH_2 + O_2 \rightarrow O{=}CHCH{=}CH_2 + HO_2 + HCHO \quad (4)$$

Under atmospheric conditions, the butadiene−OH adducts react with O_2 to form peroxy radicals that subsequently react in the presence of NO to form alkoxy radicals and NO_2.[17,22,23] The major identifiable products observed from the OH-radical-initiated oxidation of 1,3-butadiene in the presence of NO are acrolein,[19,23–26] furan,[19,22,23,26] formaldehyde,[17,25,26] 4-hydroxy-2-butenal,[26] and organic nitrates.[26] Minor products like glycolaldehyde, glycidaldehyde, 3-hydroxypropanal, hydroxyacetone, and malonaldehyde have also been observed.[17,20]

There have been relatively few measurements of the rate constant for the reaction of OH with 1,3-butadiene. Atkinson et al.[27] measured a rate constant of $(6.85 \pm 0.69) \times 10^{-11}$ cm^3 molecule^{-1} s^{-1} at 299 K and derived an Arrhenius expression of $k_1^{II}(T) = 1.45 \times 10^{-11} \exp[(930 \pm 300)/RT]$ cm^3 molecule^{-1} s^{-1} at 50 Torr in argon between 299 and 424 K using flash photolysis coupled with resonance fluorescence detection of OH radicals. Liu et al.[28] measured the rate constant for the OH + 1,3-butadiene reaction in 760 Torr of argon over the temperature range of 313−1203 K using pulse radiolysis coupled with resonance absorption detection of OH radicals, obtaining an Arrhenius expression of $k_1^{II}(T) = (1.4 \pm 0.1) \times 10^{-11} \exp[(440 \pm 40)/T]$ cm^3 molecule^{-1} s^{-1} between 313 and 623 K and a rate constant of $(6.1 \pm 0.6) \times 10^{-11}$ cm^3 molecule^{-1} s^{-1} at 313 K. Llyod et al.,[29] using a relative rate method in an environmental chamber, found the rate constant to be $(7.45 \pm 1.45) \times 10^{-11}$ cm^3 molecule^{-1} s^{-1} at 305 K. Li et al.[20] have recently reported a rate constant of $(6.93 \pm 0.48) \times 10^{-11}$ cm^3 molecule^{-1} s^{-1} at 1 Torr and 298 K using a relative rate

* To whom correspondence should be addressed. Email: iyengar@indiana.edu (S.S.I); pstevens@indiana.edu (P.S.S.).
† School of Public and Environmental Affairs.
‡ Department of Chemistry.
§ Department of Physics.

10.1021/jp8003882 CCC: $40.75
Published on Web 07/17/2008

discharge flow technique coupled with a mass spectrometer. They also obtained an Arrhenius expression of $k_1^{II}(T) = (1.58 \pm 0.07) \times 10^{-11} \exp[(436 \pm 13)/T]$ cm^3 molecule^{-1} s^{-1} at 1 Torr between 240 and 340 K, in good agreement with the previous measurements at 760 Torr, suggesting that the rate constant for the OH + 1,3-butadiene reaction is at its high-pressure limit at 1 Torr. These results are in contrast to low-pressure measurements of the OH + 2-methyl-1,3-butadiene (isoprene) reaction, which suggested that the rate constant was in the falloff region at pressures below 6 Torr and at temperatures above 343 K.[30,31] Similar results were observed for the reactions of OH with α- and β-pinene[32] and methylbutenol.[33]

The absence of an observed pressure dependence at 1 Torr for the OH + 1,3-butadiene reaction compared to that of the OH + isoprene reaction is somewhat surprising given the lower number of vibrational degrees of freedom in the OH + 1,3-butadiene reaction system compared to that of the OH + isoprene system. This paper presents the results of measurements of the rate constant for the OH + 1,3-butadiene reaction and its perdeuterated isotopomer at total pressures of 1 and 6 Torr and between 263 and 423 K using a discharge flow system coupled with laser-induced fluorescence detection (LIF) or resonance fluorescence (RF) detection of the OH radical. In addition, measurements of the rate constant for the OH + 1-butene and OH + isoprene reactions at 2−5 Torr and 300−373 K are also presented. Ab initio molecular dynamics results are presented where the intramolecular vibration redistribution is analyzed for the OH + isoprene and OH + butadiene reactions in order to gain insight into the energetics of these reactions.

II. Experimental Section

Experiments were performed using the discharge flow technique with either resonance fluorescence or laser-induced fluorescence detection of the OH radicals. Descriptions of the experimental technique have been given elsewhere.[30,34,35] The reactor consists of a jacketed 1 m long, 2.54 cm diameter Pyrex glass tube which has ports to allow for the addition of gases. A movable injector (0.3 cm o.d.) inserted in the middle of the reactor is used for the introduction of 1-butene and 1,3-butadiene. Both the tube and the injector were coated with Halocarbon wax (Halocarbon Corporation) to minimize the loss of radicals on these surfaces. Average flow velocities of approximately 10 ms^{-1} were maintained by using a Leybold D16B mechanical pump downstream of the radical detection zone. The reaction temperature was varied by circulating heated silicone oil or liquid-nitrogen-cooled ethanol through the jacket of the flow tube, and the temperature was monitored using a thermocouple located in the center of the reaction zone. Bulk flows of helium were regulated using a MKS 1179 flow controller to maintain average total pressures of approximately 1−6 Torr measured by a MKS Baratron capacitance manometer.

OH radicals were produced either by the F + H_2O → OH + HF reaction or the H + NO_2 → OH + NO reaction. Fluorine atoms were generated by a microwave discharge of CF_4 (2% in UHP He, Matheson) in the presence of He, and an excess of H_2O (<5 × 10^{13} cm^{-3}) was injected into the flow tube 2 cm downstream of the F atom source. Using this source, OH radicals were detected by laser-induced fluorescence using the $A^2\Sigma^+(v' = 1) \rightarrow X^2\Pi(v'' = 0)$ band via the $Q_1(1)$ transition near 282 nm. The excitation radiation was produced by the frequency-doubled output of a dye laser (Lambda Physik) pumped by a 3 kHz diode-pumped Nd:YAG laser (Spectra Physics). The OH A−X fluorescence near 308 nm was detected by a photomultiplier tube (Hamamatsu H 6180-01) located perpendicular to the laser radiation. A 10 nm band-pass, 20% transmissive interference filter (Esco products) centered at 308 nm was placed in front of the PMT to isolate the fluorescence from the laser scatter. The OH detection sensitivity was approximately 2 × 10^{-6} counts s^{-1} cm^3 molecule^{-1} at a laser power of 1 mW with a background signal of approximately 7000 counts s^{-1}, resulting in a minimum detectable OH concentration of approximately 2 × 10^7 molecules cm^{-3} (S/N = 1, 10 s integration).

Hydrogen atoms were generated by a microwave discharge of H_2 (99.999% Indiana Oxygen) in the presence of He, and excess concentrations of NO_2 ((2−6) ×10^{13} molecules cm^{-3}) were injected into the flow tube 2 cm downstream of the H atom source. Using this source, OH radicals were detected by resonance fluorescence using the $A^2\Sigma^+(v' = 0) \rightarrow X^2\Pi(v'' = 0)$ transition near 308 nm. The excitation radiation was produced by a microwave discharge of water in the presence of helium, and as described above, a photomultiplier tube equipped with photon counting electronics and an interference filter was used to detect the OH fluorescence at a right angle to the radiation source. Darkened baffles and light traps opposite the detector were used to reduce background scatter in the chamber. The sensitivity of this system was approximately 1 × 10^{-8} counts s^{-1} cm^3 molecule^{-1} and resulted in a minimum detectable limit of approximately 1 × 10^9 molecules cm^{-3} for OH (background signal 300−400 counts s^{-1}, S/N = 1, 10 s integration).

Heterogeneous loss of OH onto the reactor walls was observed with addition of 1,3-butadiene to the reactor as the observed pseudo-first-order decays of OH were nonlinear, leading to large positive intercepts in the second-order plots. The loss is thought to occur when OH undergoes heterogeneous reactions with the reagent adsorbed to the walls of the reactor. This behavior has previously been observed in the OH + isoprene,[30,34] α- and β-pinene,[32] methylbutenol,[33] and acetone[36] reactions. The addition of oxygen (∼2−5 × 10^{15} cm^{-3}) minimized the reagent-catalyzed loss of OH radicals on the wall of the reactor, resulting in linear and reproducible first-order decays and intercepts in the second-order plots of <10 s^{-1}. The addition of oxygen appears to reduce the reagent-catalyzed loss of OH by inhibiting active wall sites.[30,33,36,37]

Pseudo-first-order conditions were maintained during all experiments, and the OH concentrations were kept below 3 × 10^{11} molecules cm^{-3}. 1,3-Butadiene (Sigma-Aldrich, 99%) was used to prepare reagent mixtures (0.08−0.4% of 1,3-butadiene) in approximately 760 Torr of helium using either a 5.5 or 10 L calibrated reservoir fitted with a capacitance manometer. The prepared reagent was added in excess through the movable injector, and the reaction time was varied by changing the position of this injector. The concentration of the reagent was determined by measuring the pressure drop in the calibrated reservoir over time.

Pseudo-first-order decay rates (k^I_{decay}) for the OH + 1,3-butadiene reaction were obtained from the slope of the logarithm of the OH fluorescence signal versus reaction distance for a given reagent concentration under the plug flow approximation (Figure 1). The first-order decay rates were corrected for axial diffusion and OH loss on the movable injector using the following equation:

$$k^1 = k^1_{decay}\left(1 + \frac{k^1_{decay} D}{v^2}\right) - k_{injector} \quad (5)$$

Here, D is the OH diffusion coefficient in He ($0.145T^{2/3}/P$ Torr cm^2 s^{-1}), v is the average flow velocity (10.0−14.0 m s^{-1}), and $k_{injector}$ is the loss rate of OH on the movable injector,

TABLE 1: Summary of Experimental Conditions and Results for the OH + 1,3-Butadiene-h_6 and -d_6 Reactions

T (K)	[He] (10^{16} cm^{-3})	[1,3-butadiene] (10^{11} cm^{-3})	no. of exp.	k^{II} (10^{-11} cm^3 molecule^{-1} s^{-1})[a]
		OH + 1,3-Butadiene		
263	19.2–21.1	1.7–14.7	14	8.57 ± 0.42
273	17.2–18.8	3.1–21.9	12	8.24 ± 0.02
283	17.2–18.6	1.5–16.9	13	7.68 ± 0.30
300	5.4–7.9 (2 Torr)	2.2–20.8	17	6.96 ± 0.68
	8.7–10.0 (3 Torr)	1.9–24.2	16	7.01 ± 0.45
	15.8–17.7 (5 Torr)	2.4–24.7	54	6.99 ± 0.28
323	2.9	3.6–17.1	9	5.19 ± 0.82
	8.3	1.7–23.5	8	5.14 ± 1.10
	19.7	2.6–19.6	13	5.03 ± 0.56
353	2.44	2.9–24.1	10	4.79 ± 0.30
	8.5–8.8	1.5–31.2	18	4.81 ± 0.38
	16.3–16.7	4.4–38.6	17	4.77 ± 0.31
373	3.00	3.5–24.2	10	4.23 ± 0.59
	8.0	2.2–24.5	11	4.31 ± 0.23
	15.4	2.2–24.2	12	4.24 ± 0.16
393	2.3	3.1–23.8	11	4.58 ± 0.22
	6.5	2.9–28.2	10	4.46 ± 0.14
	14.6	3.3–36.3	11	4.68 ± 0.25
413	7.0	10.0–26.8	10	3.62 ± 0.44
	16.5	6.1–31.7	10	3.57 ± 0.27
423	2.3–2.7	4.3–27.9	18	3.25 ± 0.38
	7.1–7.4	6.1–35.0	17	3.15 ± 0.28
	13.5	3.3–27.7	10	3.35 ± 0.15
		OH + 1, 3-Butadiene-d_6		
300	6.5	2.2–14.2	15	6.94 ± 0.38
353	2.4	2.7–24.1	11	4.75 ± 0.28
	5.6	2.4–15.5	12	4.79 ± 0.36

[a] Uncertainties represent 2 standard deviations.

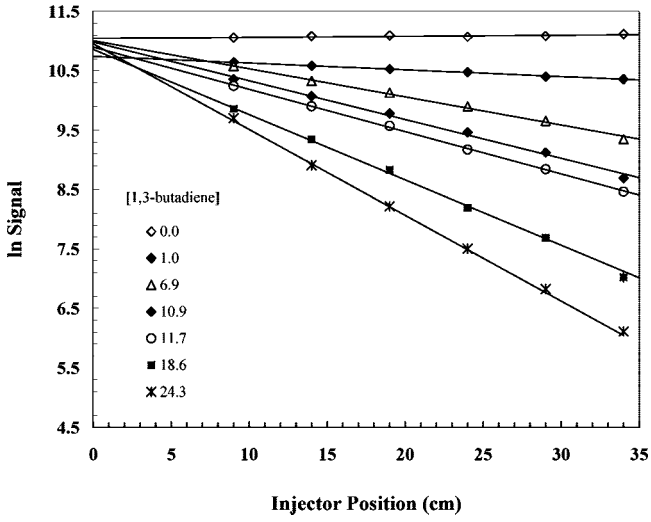

Figure 1. Sample pseudo-first-order decays of the measured OH signal for the OH + 1,3-butadiene reaction (5 Torr, 300 K). 1,3-Butadiene concentrations are in 10^{11} molecules cm^{-3}.

which was measured in the absence of 1,3-butadiene (<10 s^{-1}). The effective bimolecular rate constants (k_1^{II}) at various pressures and temperatures were calculated from a weighted linear least-squares fit of k^I versus 1,3-butadiene concentration.

III. Experimental Results

Table 1 summarizes the experimental conditions and results for reaction 1, and Figure 2 shows a plot of the observed pseudo-first-order rate constants versus the concentration of 1,3-butadiene at 300, 263, and 423 K between total pressures of 1 and 6 Torr. As can be seen from this figure, the rate constant for the OH + 1,3-butadiene reaction does not exhibit significant pressure dependence at 300 K over this pressure range. A

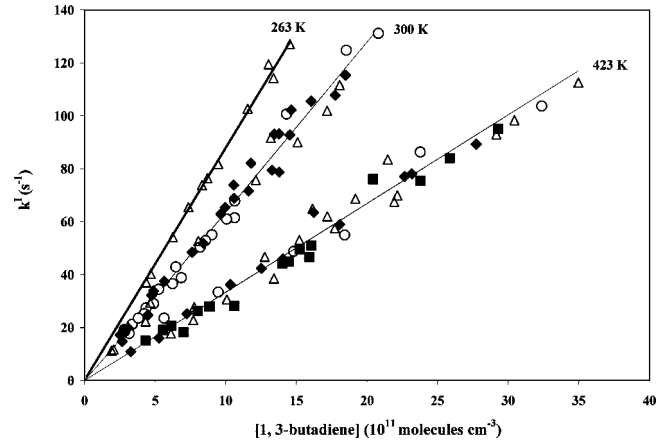

Figure 2. Second-order plot of k^I versus [1,3-butadiene] for the OH + 1,3-butadiene at 300, 263, and 423 K and between pressures of 1, 3, and 6 Torr. Open circles represent data at 2 Torr (1 Torr for 423 K), solid diamonds 3 Torr, open triangles 5 Torr, and solid squares 6 Torr.

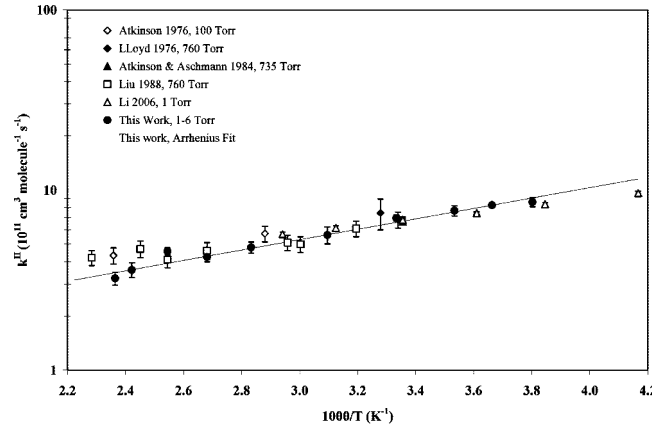

Figure 3. Arrhenius plot of the rate constants for the OH + 1,3-butadiene reaction. Uncertainties in the data represent 2 standard errors. The solid line is a weighted linear least-squares fit of the data reported in this study.

weighted linear least-square fit of the data in this plot yields a value of $k_1^{II} = (6.98 \pm 0.28) \times 10^{-11}$ cm^3 molecule^{-1} s^{-1} for the effective bimolecular rate constant at 300 K and between 2 and 5 Torr. The reported uncertainty is 2 standard errors from the precision of the weighted least-squares regression.

These results are in good agreement with previous measurements at an atmospheric pressure of $(6.1 \pm 0.6) \times 10^{-11}$ cm^3 molecule^{-1} s^{-1} at 313 K measured by Liu et al.,[28] $(7.45 \pm 1.45) \times 10^{-11}$ cm^3 molecule^{-1} s^{-1} at 305 K by Llyod et al.,[29] and $(6.65 \pm 0.21) \times 10^{-11}$ cm^3 molecule^{-1} s^{-1} at 295 K by Atkinson and Aschmann.[38] They are also in excellent agreement with the rate constant of $(6.85 \pm 0.69) \times 10^{-11}$ cm^3 molecule^{-1} s^{-1} measured by Atkinson et al.[27] in 50 Torr of argon using the flash photolysis−resonance fluorescence technique and with measurements obtained at 1 Torr by Li et al.,[20] who observed a rate constant of $(6.83 \pm 0.24) \times 10^{-11}$ cm^3 molecule^{-1} s^{-1} using a relative rate discharge flow technique.

The temperature dependence at various pressures for the OH + 1,3-butadiene was measured between 263 and 423 K, and the results are also summarized in Table 1 and Figures 2 and 3. As can be seen from Figure 2, the rate constant for the OH + 1,3-butadiene reaction does not exhibit significant pressure dependence over the temperature and pressure range studied. A weighted fit of the rate constants as a function of temperature

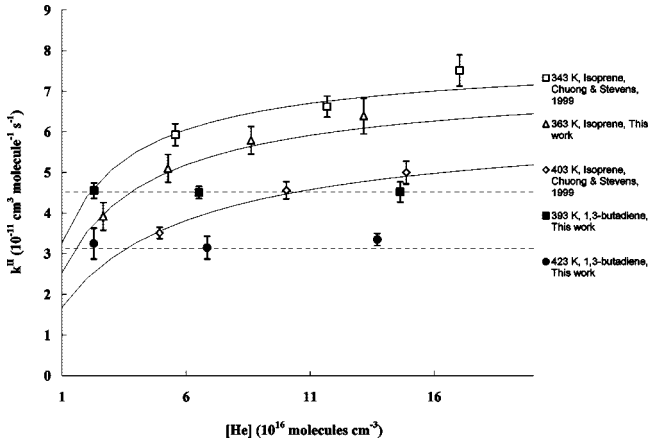

Figure 4. Plot of k^{II} versus [He] at temperatures in the range of 343−423 K for the OH + isoprene reaction and at 393 and 423 K for OH + 1,3-butadiene reaction. Uncertainties in the data represent 2 standard errors. The solid lines are the weighted least-squares fittings of the falloff behavior of isoprene (ref 29). The dashed lines correspond to the average rate constants at 393 and 423 K for the OH + 1, 3-butadiene reaction between total pressures of 1 and 6 Torr.

(Figure 3) yields the following Arrhenius expression for reaction 1, with the uncertainty representing 2 standard errors from the weighted fit:

$$k^{II}(T) = (7.23 \pm 1.2) \times 10^{-12} \exp(664 \pm 49/T)\ \text{cm}^3\ \text{molecule}^{-1}\ \text{s}^{-1}$$

The observed negative activation energy ($E_a/R = -664$ K) is in reasonable agreement with the value of $E_a/R = -440$ K obtained by Li et al.[20] and the value of $E_a/R = -470$ K obtained by Atkinson et al.[27]

The negative temperature dependence observed for the OH + 1,3-butadiene reaction is consistent with a reaction mechanism that is dominated by OH addition to the double bond through the formation of a long-range complex[39] rather than by H-abstraction even at the low pressures and high temperatures of these experiments. Although the negative temperature dependence and absence of a pressure dependence could indicate a hydrogen-abstraction mechanism through a pre-reactive complex, similar to that observed in the OH + acetic acid reaction,[40] previous measurements of the products of the OH + 1,3-butadiene reaction and theoretical calculations of the potential energy surface suggest that H-abstraction is a minor product channel.[20,27,28] Indeed, our measurement of the rate constant of the reaction of OH and 1,3-butadiene-d_6 did not exhibit a kinetic isotope effect at a temperature of 363 K and pressure of 1 Torr ($k^{II}(D) = (4.79 \pm 0.4) \times 10^{-11}$ cm^3 molecule^{-1} s^{-1}; $k^{II}(H) = (4.75 \pm 0.3) \times 10^{-11}$ cm^3 molecule^{-1} s^{-1}), suggesting that OH addition dominates the mechanism for this reaction even at the low pressures and high temperatures of these experiments.

The agreement between the rate constants measured at low pressures (1, 3, and 6 Torr) reported here with those measured at higher pressures suggests that over the temperature range in this study, the OH + 1,3-butadiene reaction has reached its high-pressure limit at pressures as low as 1 Torr (Figures 3 and 4), consistent with the results of Li et al.[20] at 1 Torr and between 240 and 340K. These results suggest that the hydroxyalkyl radical formed from the OH addition to 1,3-butadiene can easily distribute the excess energy resulting from the electrophilic addition of OH to one of the double bonds in 1,3-butadiene and stabilize the adduct with a minimal number of third-body collisions. At higher temperatures, the rate of stabilization of the adduct is still greater than the rate of thermal dissociation.

TABLE 2: Summary of Experimental Conditions and Results for the OH + 1-Butene and OH + Isoprene Reactions

T (K)	[He] (10^{16} cm^{-3})	[1-butene] (10^{11} cm^{-3})	no. of exp.	k^{II} (10^{-11} cm^3 molecule^{-1} s^{-1})[a]
		OH + 1-Butene		
300	7.2	2.7–23.3	11	3.05 ± 0.18
	9.0	5.4–20.7	13	3.16 ± 0.13
	16.8	3.5–40.2	11	3.03 ± 0.14
353	5.9	7.3–50.8	10	2.28 ± 0.13
	9.0	6.8–45.5	10	2.31 ± 0.26
	14.3	11.3–82.8	10	2.23 ± 0.25
373	5.4	6.7–41.5	10	2.03 ± 0.32
	7.5	9.7–55.0	10	2.07 ± 0.24
	13.0	10.7–65.3	11	2.00 ± 0.22
		OH + Isoprene		
300	16.1	1.9–16.6	13	10.24 ± 0.62
363	2.8	1.3–15.4	12	3.92 ± 0.52
	5.3	4.0–18.3	10	5.06 ± 0.44
	8.6	1.6–16.6	10	5.74 ± 0.56
	13.2	0.98–17.0	13	6.15 ± 0.36

[a] Uncertainties represent 2 standard deviations.

In contrast, the rate constants for the reactions of OH with isoprene and methyl butenol do exhibit a pressure dependence above room temperature, which had previously been attributed to an increase in the rate of thermal dissociation of these adducts at higher temperatures competing with the rate of stabilization, leading to an observed falloff of the rate constant at low pressure. To improve confidence in these measurements, the rate constants for the reactions of OH with isoprene and 1-butene were also measured between 300 and 375 K and 1 and 6 Torr. These results are summarized in Table 2 and in Figure 4.

The measurements reported here of the rate constant for the OH + 1-butene reaction of $k^{II} = (3.03 \pm 0.14) \times 10^{-11}$ cm^3 molecule^{-1} s^{-1} at 300 K and are in good agreement with the value of $(3.53 \pm 0.36) \times 10^{-11}$ cm^3 molecule^{-1} s^{-1} at 299 K and 50 Torr of argon reported by Atkinson and Pitts[41] using flash photolysis coupled with resonance fluorescence detection of OH radicals and the value of $(3.03 \pm 0.34) \times 10^{-11}$ cm^3 molecule^{-1} s^{-1} at 297 K and 20 Torr using a pulsed laval nozzle coupled with LIF detection of OH reported by Vakhtin et al.[42] The results reported here are larger than the value of $(1.5 \pm 0.1) \times 10^{-11}$ cm^3 molecule^{-1} s^{-1} reported by Pastrana and Carr[43] using discharge flow and line absorption photometry detection of OH radicals.

A weighted linear least-squares fit of the rate constants as a function of inverse temperature for the OH + 1-butene reaction results in an Arrhenius expression of $k^{II}(T) = (4.6 \pm 0.78) \times 10^{-12} \exp((559 \pm 52)/T)$ cm^3 molecule^{-1} s^{-1} for the temperature dependence of the rate constant, where the uncertainties represent 2 standard errors from the fit. The negative activation energy (−1.1 kcal mol^{-1}) derived from the above expression is similar to that (−0.93 kcal mol^{-1}) obtained by Atkinson and Pitts,[41] who reported an Arrhenius expression of $7.6 \times 10^{-12} \exp[(930 \pm 300)/RT]$ cm^3 molecule^{-1} s^{-1}.

Similar to the results for the reaction of OH with 1,3-butadiene, the agreement between the rate constants measured at room temperature and low pressures (2, 3, and 5 Torr) with those measured at higher pressures suggests that the OH + 1-butene reaction is at its high-pressure limit at 2 Torr, even at temperatures higher than room temperature. In contrast, the results for the OH + isoprene reaction (Table 2 and Figure 4) show a pressure dependence above room temperature and agree well with previous studies at low pressure.[30,31]

IV. Discussion of Experimental Results

There have been several studies of the pressure and temperature dependence of the OH addition to various unsaturated organic compounds under low-pressure conditions. Although the OH + ethene reaction exhibits a pressure dependence at room temperature and pressures less than 10 Torr,[30,44] the OH + isoprene, α- and β-pinene, methyl vinyl ketone, and methyl butenol reactions generally do not exhibit a pressure dependence at room temperature, with the measured rate constants at low pressure in good agreement with measurements at higher pressures. This suggests that these reactions are still at their high-pressure limits at room temperature and at pressures as low as 2 Torr. However, above room temperature, the rate constants for these reactions do exhibit a pressure dependence at low pressures (2−6 Torr).[30−33,35]

These results would suggest that the excess energy due to the addition of OH to the double bond of isoprene, methyl vinyl ketone, methyl butenol, and other >C4 alkenes is easily distributed through the large number of available vibrational degrees of freedom, and the excited adducts are stabilized quickly with a minimal necessary number of third-body collisions. However, at higher temperatures, the rate of thermal dissociation of the HO adducts increases and begins to compete with the rate of stabilization, leading to an observed falloff of the rate constant at low pressure.

Although the pressure range in this study is limited, the absence of an observed pressure dependence at higher temperatures for the OH + 1,3-butadiene reaction is somewhat surprising given the fewer vibrational degrees of freedom available to distribute the excess energy associated with OH addition compared to the larger isoprene and methyl butenol reaction systems. The absence of an observed pressure dependence for the OH + 1,3-butadiene reaction could indicate the presence of a hydrogen-abstraction channel that becomes important at low pressure. For example, no significant pressure dependence was observed for the rate constant for the OH + methacrolein reaction between 2 and 5 Torr and over the temperature range of 300−422 K.[35] In contrast to the other OH + alkene reactions discussed above, abstraction of the aldehydic hydrogen in the OH + methacrolein reaction occurs in addition to OH addition, with a branching ratio of approximately 50%.[45,46] The absence of an observed pressure dependence for the OH + methacrolein reaction suggested that the H-atom-abstraction channel for this reaction dominates the overall rate constant for the OH + methacrolein reaction at higher temperatures.[35,47] However, our measurements of the rate constant of the reaction of OH and 1, 3-butadiene-d_6 did not exhibit a significant kinetic isotope effect even at a temperature of 363 K and pressure of 1 Torr, suggesting that H-abstraction is not occurring to a significant extent under these experimental conditions (Table 1).

One possible explanation for the observed difference in the pressure dependences for the OH + 1,3-butadiene and OH + isoprene reactions is a difference in stabilization energies of the OH-addition products for these reactions. A higher stabilization energy for the HO−isoprene adducts compared to that for the HO−butadiene adducts could require more third-body collisions at higher temperatures to remove the excess energy upon OH addition. However, previous ab initio studies of the OH + 1,3-butadiene and the OH + isoprene reactions suggest that the stabilities of the products are similar, with OH addition to the terminal carbons producing adducts that are more stable than addition to the internal carbons. For the OH + 1,3-butadiene reaction, Li et al.[20] found that addition to the terminal carbons produced adducts that were 29.3−36.4 kcal/mole more stable than the reactants at the PMP4/6-311++G(d,pd)//MP2/6-311++G(d,p) level of theory, while addition to the internal carbons were 15.7−19.6 kcal/mole more stable than the reactants. Similar results were found for the OH + isoprene reaction, where addition to the terminal carbons was found to be 35.4−37.9 kcal/mole more stable than the reactants at the PMP4/6-311G(d,p)//MP2/6-311++G(d,p) level of theory, while addition to the internal carbons was found to be 24.2−25.6 kcal/mole more stable than the reactants.[48] These results suggest that the lack of a pressure dependence for the OH + 1,3-butadiene reaction may not be due to a significant difference in the stabilization energy of the products of the reaction.

However, the observed difference in the pressure dependences for the OH + 1,3-butadiene and 1-butene reactions with the OH + isoprene reaction may reflect a difference in reactivity of the hydroxyalkyl radicals formed from OH addition. The lack of an observed pressure dependence for the OH + 1,3-butadiene reaction may suggest that the reaction of the hydroxyalkyl radical products with O_2 to form hydroxyl alkyl peroxy radicals may be faster than that for the OH + isoprene reaction, reducing the lifetime of the hydroxyalkyl radicals. As a result, the decomposition of the hydroxyalkyl radicals leading to the formation of reactants may not be able to compete with both stabilization and reaction with O_2, leading to an observed absence of a pressure dependence for the OH + 1,3-butadiene reaction and similarly for the OH + 1-butene reaction. These results suggest that the observed pressure dependence for the OH + isoprene,[30] α- and β-pinene,[32] methyl vinyl ketone,[35] and methyl butenol[33] reactions at elevated temperatures may not solely reflect low-pressure falloff behavior but may reflect a competition between dissociation of the adduct and reaction with O_2 to form more stable peroxy radicals. However, similar pressure dependences measured in the absence of added oxygen have been observed for the OH + 1,3-butadiene and OH + isoprene reactions, suggesting that the observed pressure dependence may not depend on the oxygen concentration in the system.[20,49] Clearly, additional measurements are needed to resolve this discrepancy.

Another possible explanation for the lack of an observed pressure dependence for the OH + butadiene and 1-butene reactions compared to the OH + isoprene reaction at low pressures and temperatures above room temperature may be related to the pathways available for dissipation of energy in the hydroxyl−alkyl adducts, that is, the rate of intramolecular vibrational redistribution (IVR). We probe the available pathways for energy dissipation in greater detail in the next section using ab initio molecular dynamics. Indeed, for all reactions that culminate in the formation of a unimolecular product, energy dissipation is critical; the number of modes available for redistribution of energy raises the entropic and thus free energetic stability of the product. Such an energy dissipation process, while generally facilitated by termolecular collision processes, is forced to remain an intramolecular process under low-pressure conditions. In the next section, we investigate the mechanism of IVR for the hydroxyl−alkyl adducts corresponding to 1,3-butadiene and isoprene.

V. Analysis of Intramolecular Energy Transfer and Dynamically Averaged Vibrational Properties through Ab Initio Molecular Dynamics Simulations

To gauge the vibrational energy transfer in butadiene−OH adducts and to compare it with that of isoprene−OH adducts, we present preliminary results obtained using ab intio molecular

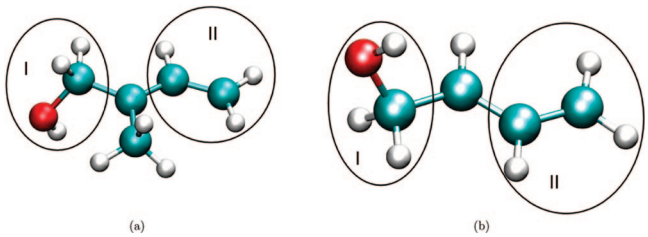

Figure 5. Structure of (a) isoprene−OH and (b) butadiene−OH adducts showing the three fragments for AIMD simulations.

dynamics (AIMD) methodologies, atom-centered density matrix propagation (ADMP),[50–55] and Born Oppenheimer molecular dynamics (BOMD).[56–59] These simulations utilized the B3LYP hybrid density functional with double-zeta polarized-diffused 6-31+G(d,p) basis, as suggested from previous studies on similar systems.[52,54,55,60–66] In addition, geometry optimizations and harmonic frequency calculations at the B3LYP level and post-Hartree Fock MP2 levels using triple-zeta 6-311++G(d,p) Gaussian basis were performed to confirm and benchmark results.[67] AIMD techniques, such as ADMP and BOMD, have recently been utilized in many state-of-the-art studies to obtain dynamically averaged, temperature-dependent, vibrational properties of weakly bound hydrogen-bonding clusters.[54,55,60–63,68,69]

V(a). Simulation Details. All simulations were conducted using a development version of the Gaussian series of electronic structure codes.[70] To understand vibrational energy transfer, the AIMD simulations were conducted starting from initial configurations that provided an asymmetric distribution of kinetic energies for the individual atoms. These kinetic energies were assigned to the individual atoms based on the results from an initial geometry optimization and harmonic frequency calculation of butadiene− and isoprene−OH adducts. Following this, a linear combination of normal mode vectors was constructed to provide greater initial kinetic energies to certain fragments in the molecule. (This aspect is discussed below in greater detail.) A time step of 0.4 fs was chosen for all BOMD dynamics studies, while a fictitious mass-tensor[47] scaling value of 0.1 amu bohr^2 ($\approx$180 au) and a time step of 0.25 fs was used for ADMP. All AIMD simulations conducted here are microcanonical (NVE), with acceptable fluctuations (noted below) in the internal temperature. Since time correlation functions involving nuclear velocities as well as molecular dipoles are utilized here to obtain vibrational properties, a constant energy simulation with an associated conserved Hamiltonian corresponding to the real system is critical. Finite temperature dynamically averaged vibrational spectra and the vibrational density of states were computed using Fourier transform of the nuclear velocity (represented as FT-VAC) and dipole (FT-DAC) autocorrelation functions in order to probe the vibrational energy transfer. All simulations for the hydroxyl−isoprene adduct presented here had an average temperature of 227 $\pm$ 37 K, whereas the average temperature for the hydroxy−butadiene simulations were 246 $\pm$ 55 K. (Note that both temperature and energy cannot be exactly conserved during molecular dynamics simulations.) The temperature of the molecular cluster systems studied here was computed using the equipartition theorem, that is, the kinetic energy from the simulations, computed using the nuclear velocities, was assumed to be equal to $3/2(N-1)kT$, where N is the number of atoms in the system. This approximation has been found to provide reasonable approximations to cluster temperature for a variety of ADMP studies.[52,54,55,60–65]

The vibrational-energy-transfer mechanism was probed by considering (a) the evolution of the Fourier transform of the velocity−velocity autocorrelation function (FT-VAC) as a function of time for the full molecule as well as the individual fragments, (b) a detailed analysis of the evolution of contributions from the individual Harmonic modes (to be discussed in section VI(c)) as a function of time, and (c) the evolution of the individual fragment kinetic energies as a function of time. It must be noted that the FT-VAC provides a representation of the vibrational density of states sampled during finite temperature simulations.

For the four isoprene−OH adducts, we divide the molecule into three fragments; the terminal methylene group to the left of the C−CH_3 is labeled as fragment I, the vinyl group to the right is labeled as fragment II, and the C−CH_3 is labeled as fragment III, with the OH present on either of the fragments depending on the adduct (see Figure 5a). For the butadiene−OH adducts, we divide the system similarly into three fragments, a terminal methylene group labeled I, a terminal vinyl group labeled II, and the C−H group, labeled III (see Figure 5b). In the first adduct, OH is present on one of the terminal methylene groups, while in the second adduct, the OH is attached to one of the two central C−H carbon atoms. Using these fragments, OH can either be attached to fragment II or fragment III for the second adduct, giving two distinct adducts for initial kinetic energy considerations.

We use a linear combination of the normal mode vectors corresponding to the C−H and O−H stretch from the harmonic frequency analysis to construct an asymmetric distribution of kinetic energies for the atoms such that fragment III has the lowest total kinetic energy and two initial configurations with either fragment I or fragment II with the highest kinetic energy. Thus, two initial configurations for each adduct resulting in a total of eight configurations for isoprene−OH adducts and six configurations for butadiene−OH adducts were subjected to ADMP and BOMD simulations for dynamics up to 20 ps each utilizing the B3LYP hybrid density functional with double-zeta polarized-diffused 6-31+G(d,p) basis. In the current work, we report results from ab initio dynamical simulations for adduct 1 of both isoprene and butadiene with the highest kinetic energy in fragment I. Additional discussions on simulations on all adducts will be part of a future publication.[67] Furthermore, results from ADMP and BOMD are qualitatively similar, and hence, only ADMP results are presented here.

V(b). Analysis of Structural, Dynamical, and Spectroscopic Properties from ADMP Simulations. The three fragments start with different kinetic energies and equilibrate during the simulations (Figure 6) via transfer of energy between the vibrational modes. In Figure 6, we present the time evolution of a kinetic energy quotient, which is defined as the ratio of the kinetic energy per atom for each fragment to the kinetic energy per atom of the whole molecule. This quotient has the physical interpretation that when it is equal to one, the average kinetic energy in the fragment is equal to that in the molecule. We notice in Figure 6 that the kinetic energy quotients for all three fragments equilibrate towards unity. Furthermore, although it appears from Figure 6 that the isoprene adducts equilibrate faster compared to butadiene adducts, the results presented here are for a single trajectory; hence the equilibration process between the different fragments does not provide a complete description of the rate of energy transfer. It does however provide valuable insight into the mechanism of energy flow via intramolecular vibrational energy redistribution, which we analyze here.

To understand the mechanism of energy flow in the two systems, we computed the FT-VAC function at intervals of 2 ps. As a result of our simulations, we find that there is a distinct

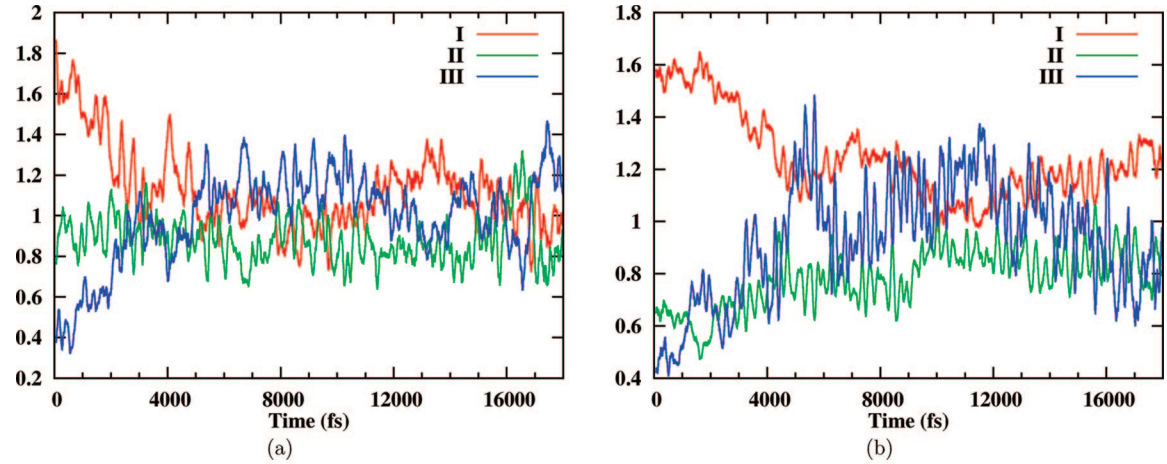

Figure 6. Time evolution of the kinetic energy quotients (see text) of the three fragments for adduct 1 of (a) isoprene−OH and (b) butadiene−OH for an initial configuration with the kinetic energy of fragment I greater than that of fragment II. Further details on the vibrational modes that participate in the equilibration process can be seen in Figures 10–12. The time evolutions of the kinetic energies and those of the proton and OH distance (Figure 7) support the presence of a five-membered ring and its role in the energy-transfer pathway mechanism in OH + isoprene.

difference between the energy-transfer pathways in isoprene and butadiene. In Figure 7, we present the FT-VAC spectrum, that is, the vibrational density of states, at 18 ps for adduct 1 of both isoprene−OH and butadiene−OH from ADMP simulations

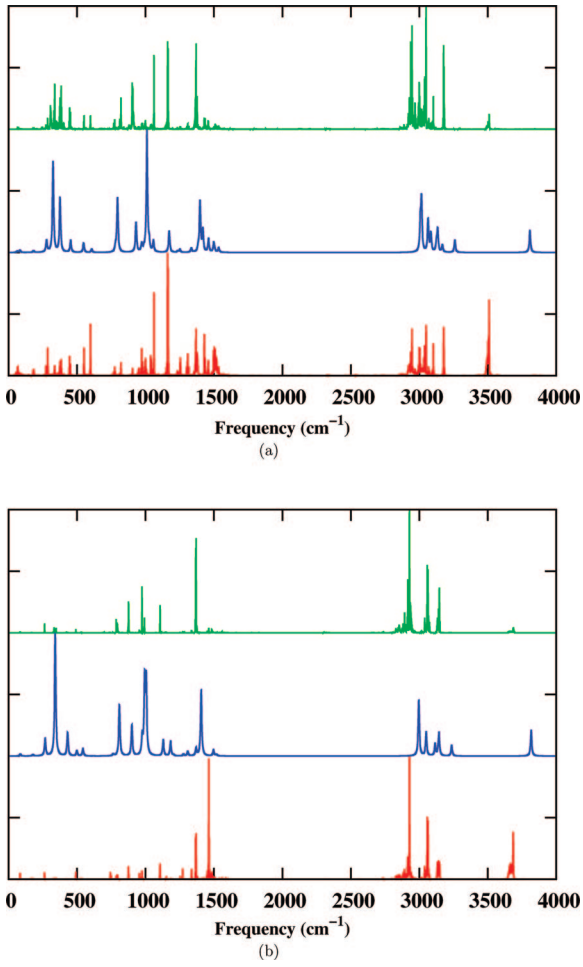

Figure 7. Comparison of the Fourier transform velocity−velocity autocorrelation function (red) and the Fourier transform dipole autocorrelation function (green) at 18 ps with the IR spectrum obtained from a harmonic frequency analysis (blue) for (a) isoprene−OH and (b) butadiene−OH adducts. Note the large shift in the OH stretch peak in isoprene−OH due to anharmonicity. See text for details.

and compare them with those obtained from the harmonic frequency obtained at the optimized geometries. In addition, we also provide the Fourier transform of the dipole autocorrelation function (FT-DAC) here since this includes the infrared dipole selection rules. The spectrum can be characterized into three distinct frequency ranges: (1) >3400 cm^{-1}, the OH stretch region, (2) 2700−3400 cm^{-1}, the C−H stretch, and (3) 0−1800 cm^{-1}, the C−O and C−C stretches and the various bending modes.

The harmonic spectra and the dynamically averaged FT-VAC and FT-DAC are generally in agreement except at the OH stretch peaks in isoprene−OH and butadiene−OH. Note that these anharmonic frequencies are not obtained by correcting the harmonic frequencies as is done in standard calculations[71] but are instead captured completely through sampling the potential surface as it is calculated within finite temperature AIMD simulations. The AIMD simulations show an anharmonicity correction to the OH stretch of approximately 200−300 cm^{-1} in the isoprene adducts and 100−200 cm^{-1} in the butadiene adducts. To further examine the reason behind the large anharmonic contribution in isoprene, we performed a potential energy scan of the OH distance at the equilibrium geometry of isoprene and found the potential to have contributions up to fourth order. The anharmonicity correction to the C−H stretching vibrational modes is small compared to that of the O−H stretching mode. The appearance of a large anharmonicity in the O−H stretching mode is further accentuated by the formation of stable five-membered ring-like conformers in the case of isoprene, with the OH oxygen donating its lone pairs to the CH protons.

The difference in the formation of five-membered rings in the isoprene−OH adduct compared to that in the butadiene−OH adduct can be seen in Figure 8, where we show the time evolution of the distance between the OH oxygen atom and the CH protons and the radial distribution functions for the same. In the isoprene−OH adduct, all three H atoms in the methyl group are considered. (The three protons are represented by different colors in Figure 8a to observe the constrained rotation of the methyl group about the C−C bond. For free rotation of the methyl group, the probability of the distance of each proton from the oxygen atom would be the equal and the three protons indistinguishable for spectral considerations). From Figure 8a, it appears that the methyl group undergoes rotation with at least

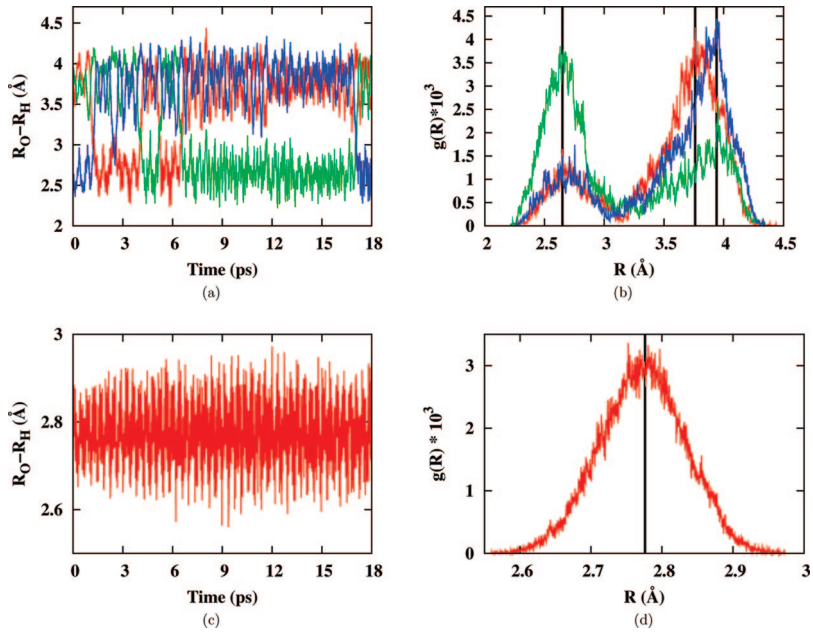

Figure 8. (a) Time evolution of the distance between the OH oxygen atom and methyl protons of isoprene during the dynamics and (b) plots of the corresponding radial distribution function, $g(R)$, of the methyl protons from the oxygen atom. (c) Distance between the oxygen atom and CH proton of butadiene during the dynamics and (d) the corresponding radial distribution function, $g(R)$. The solid vertical lines in (b) at 2.65, 3.76, and 3.94 Å and that in (d) at 2.78 Å show the most probable distance between the proton and oxygen in isoprene and butadiene, respectively.

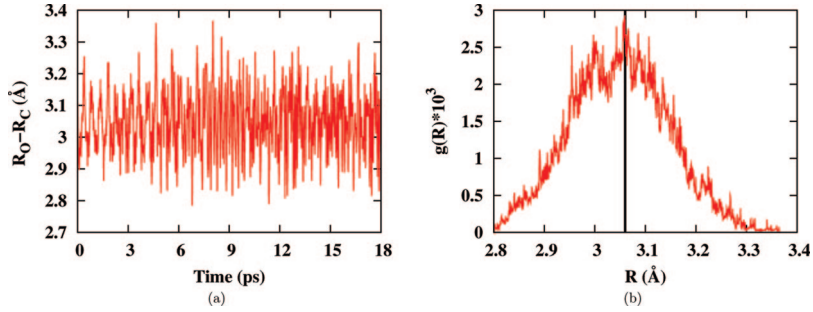

Figure 9. (a) Time evolution of the distance between the OH oxygen atom and methyl carbon of isoprene during the dynamics and (b) a plot of the corresponding radial distribution function, $g(R)$, of the methyl carbon from the oxygen atom. The solid vertical line in (b) at 3.06 Å shows the most probable distance between the carbon and oxygen in isoprene.

one proton remaining at a distance of ~2.65 Å from the oxygen atom while the other protons are approximately 3.8 Å from the oxygen atom. This is also seen from the corresponding radial distribution function (RDF) in Figure 8b, which gives the probability of the distance between the oxygen and methyl proton during the dynamics simulation, with the vertical lines at 2.65, 3.76, and 3.94 Å showing the most probable distance between the proton and oxygen atom. Similarly, a geometry optimization at the B3LYP/6-31+G(d,p) level of theory gives distances of 2.66, 3.83, and 3.82 Å between the oxygen and the methyl protons. Also, the angle between the OH bond and an imaginary line joining the oxygen to the closest methyl proton is 103°, from which we can conclude that the lone pair on the oxygen atom is pointing toward the methyl proton, forming a five-membered O−C−C−C−H ring that is preserved even during finite temperature simulations. In the butadiene−OH adduct, the most probable distance between the proton and oxygen is 2.78 Å, as seen from the vertical line in the RDF in Figure 8d, but the corresponding angle is 90°, which hinders formation of an optimally oriented ring similar to that in the isoprene−OH adduct.

To further support the presence of a five-membered ring structure in the isoprene−OH adduct, we show the time evolution of the distance between the oxygen atom and the methyl carbon in Figure 9a and its corresponding RDF in Figure 9b. The most probable distance between the oxygen and carbon is 3.06 Å, with some fluctuation during the dynamics. Thus, there are two basic reasons for the large anharmonic red shift in the OH stretch frequency of the isoprene−OH adduct. First, the intrinsic anharmonicity for the OH stretch is different for the isoprene−OH adduct as compared to that for the butadiene−OH adduct, and this aspect is gauged by performing a potential energy scan of the OH proton as discussed above. However, second, and more importantly, the OH oxygen in the isoprene adduct can be involved in stable five-membered rings that are retained even during finite temperature ab initio dynamics. These five-membered rings are characterized by a lone pair donation from the OH oxygen toward a methyl proton. This process weakens the associated OH bond stretch and results in its red shift. Such a shift in the frequency is to be distinguished from the large number of OH stretch red shifts that have been recently reported in the literature for hydrogen-bonded systems.[61–63,72–74] While in all of those cases it was the hydroxyl proton that was involved through active hydrogen bonding leading to a shift in frequency, in the case of isoprene−OH, it is the lone pair electrons associated with the oxygen, the donation of which to nearby protons leads to a red shift.

These ring formations, as we note in the next section, are also responsible for energy transfer from the OH and CO stretch modes into the various CH bend and wag modes of the adduct molecules. We arrive at these conclusions based on a decomposition of the dynamically averaged spectra in terms of the harmonic normal modes to determine the modes responsible for energy redistribution.

V(c). Vibrational Energy Transfer from FT-VAC Calculations. We have recently introduced a scheme to decompose and assign the finite temperature vibrational density of states utilizing Harmonic normal mode vectors.[69] We briefly summarize here the key equations involved in the decomposition process and adapt this technique to provide an analysis tool for vibrational energy transfer. As per the convolution theorem,[75] the FT-VAC may be written as a power spectrum of the Fourier transform of the mass-weighted velocity vectors

$$\tilde{V}^{t'}_{j,k}(\omega) = \int_0^{t'} \mathrm{d}t \exp[-i\omega t] V_{j,k}(t) \quad (6)$$

where $V_{jk}(t)$ is the kth mass-weighted velocity component for the jth atom. Since mass-weighted normal mode vectors are eigenstates of the Hessian matrix and hence form a complete orthonormal set, we can expand $\vec{\tilde{V}}^{t'}(\omega)$ in such a basis as follows:

$$\vec{\tilde{V}}^{t'}(\omega) = \sum_i C_i^{t'}(\omega) * \vec{H}_i(\omega) \quad (7)$$

where H_i is the ith Harmonic (mass-weighted) normal mode vector. The expansion coefficients, $C_i(\omega) = \vec{H}\,\vec{\tilde{V}}^{t'}(\omega)$ in eq 7, are then the contribution of the ith normal mode vector to the Fourier transform of the velocity in eq 6 at frequency ω for a MD simulation of length t'. The net contribution of the ith normal mode to the vibrational density of states in the frequency range $[\omega_1, \omega_2]$ may then be written as a superposition of all of its contributions inside of the frequency range

$$C^{\Delta\omega}_{i,t'} = C^{[\omega_1,\omega_2]}_{i,t'} = \left[\int_{\omega_1}^{\omega_2} \mathrm{d}\omega |C_i^{t'}(\omega)|^2\right]^{1/2} = \left[\int_{\omega_1}^{\omega_2} \mathrm{d}\omega |\vec{H}_i \cdot \vec{\tilde{V}}^{t'}(\omega)|^2\right]^{1/2} \quad (8)$$

By estimating the predominant contribution from the projection of the FT-VAC onto the normal modes, additional insight into the intramolecular vibrational redistribution can be obtained. The t'-dependent evolution of the critical harmonic components over a range of frequencies of interest provides insight into the mechanism of intramolecular vibrational energy transfer and redistribution.

In Figures 10−12, we show the evolution of the most dominant modes for the butadiene−OH and isoprene−OH adducts. From Figure 10, we note that the predominant exchange of energy in the butadiene−OH adduct occurs on a 10−18 and a 2−6 ps time scale. The characteristic modes that are involved in these two processes are quite different. For example, over the short time scale (2−6 ps), we find that energy leaks out of the O−C1−C2 wag mode (described by the Harmonic mode ν_1 in Figure 10a and b) and into a CO stretch coupled with the bending of the C−C backbone motion (described by ν_2 in Figure 10a and c). Over the longer time scale (10−18 ps), energy leaks out of a backbone (C1−C2−C3−C4) bending mode coupled to a torsional motion of the O−C1−C2 atoms (described by ν_3 in Figure 10a and d) and into an open jaw O−C1−C2 motion which is coupled to the C−C stretch of the backbone with appropriate motion of the attached H atoms. From Figure 12, we also note that there is longer time scale (8−18 ps) exchange between the ν_1 and ν_5 modes. Figure 12 further depicts exchange between the CO stretch mode (described by ν_{13} in Figure 12a and c) and an umbrella motion of the attached H atoms. It is already indicative that the hydrogen bonded to the C2 atom of butadiene participates, albeit weakly, in energy transfer through its interaction with the OH oxygen.

This participation is further enhanced in the case of isoprene, where the C−H proton at the C2 position of butadiene is replaced by a methyl group which provides a higher degree of interaction based on the presence of a five-membered ring discussed before. In fact, the five-membered ring forms the basis of all energy exchanges in the isoprene−OH adduct, where we also note a loss of energy from the open jaw motion of the five-membered ring (described by ν_8 in Figure 11a and c). As a result of these ring formations, it appears that the mechanism of intramolecular vibrational energy transfer and redistribution in the OH + isoprene reaction is significantly different than that in the OH + butadiene reaction. The fundamental effect thus arises from the higher anharmonicity intrinsically present in the isoprene−OH bond, as indicated by AIMD simulations. For this same reason, isoprene−OH is also more likely to interact with neighboring molecules through the anharmonic OH oxygen and hydrogen atoms, thus enhancing the effect of energy flow as pressure increases. As a result, one might

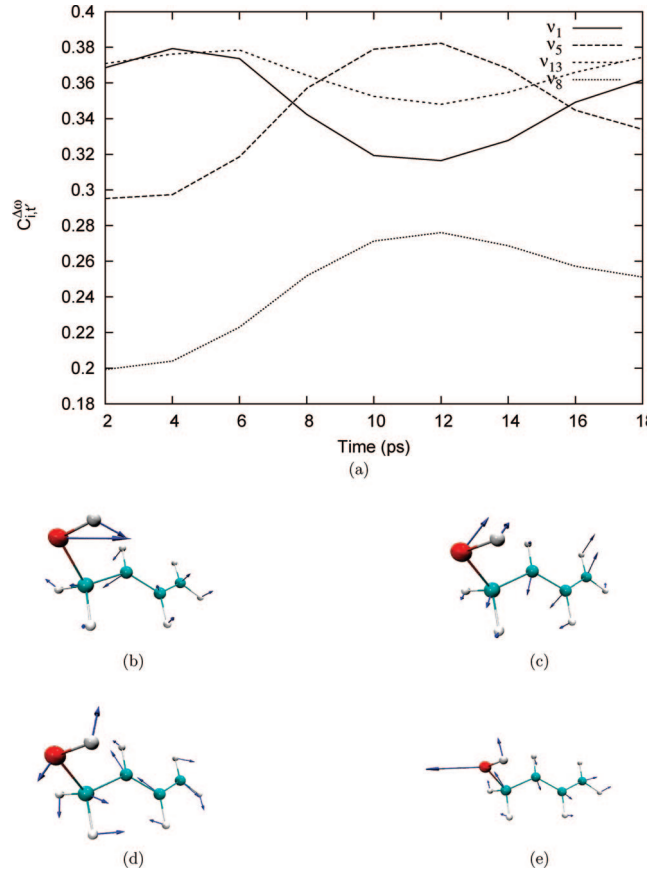

Figure 10. (a) The t'-dependent evolution of the harmonic components, $Ci,t'^{\Delta\omega}$, of the butadiene−OH adduct 1 in the frequency range of $\Delta\omega$ = [1200−1800] cm^{-1}. Harmonic modes (b)ν_1, (c) ν_2, (d) ν_3, and (e) ν_5 correspond to the four dominant modes. The modes ν_1 and ν_2 represent torsional motions about the C1−C2 single bond that exchange energy, while ν_3 and ν_5 represent orthogonal wags of the entire network about the C1−C2 bond.

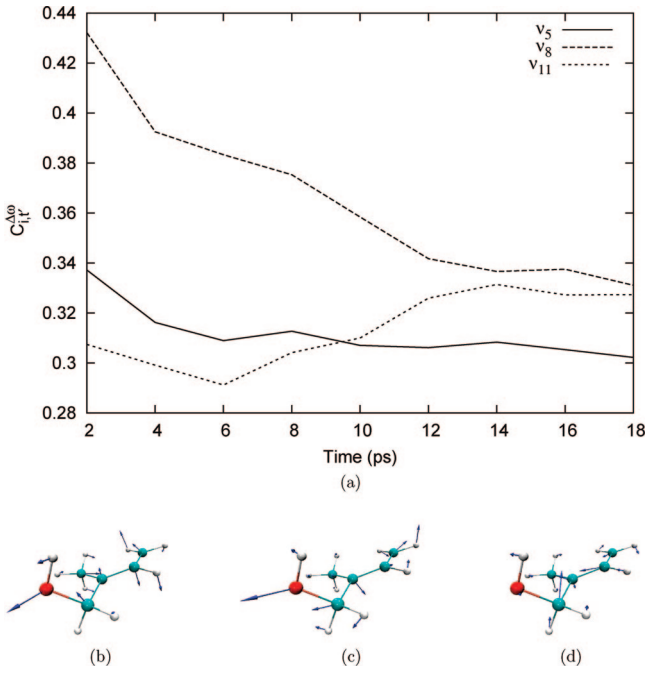

Figure 11. (a) The t'-dependent evolution of the harmonic components, $Ci,t'^{\Delta\omega}$, of the isoprene−OH adduct 1 in the frequency range of $\Delta\omega = [1200-1800]$ cm^{-1}. Harmonic modes (b) ν_5, (c) ν_8, and (d) ν_{11} correspond to the dominant modes. The plots indicate that an energy exchange from ν_5 and ν_8 to ν_{11} involves the open jaw motion of the five-membered O−C−C−C−H ring.

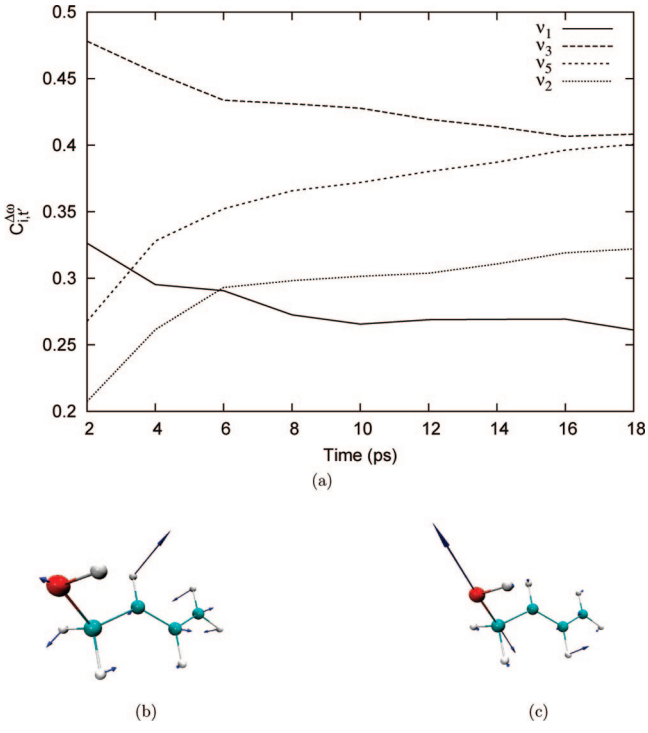

Figure 12. (a) The t'-dependent evolution of the harmonic components, $Ci,t'^{\Delta\omega}$, of the butadiene−OH adduct 1 in the frequency range of $\Delta\omega = [1200-1800]$ cm^{-1}. Harmonic modes (b) ν_8 and (c) ν_{13} correspond to the dominant modes. The mode ν_{13} involves the CO stretch, whereas ν_8 involves a major wag contribution from the hydrogen attached to the second carbon (C2). See Figure 10b for ν_1 and Figure 10e for the ν_5 mode.

expect the kinetics of the OH + isoprene reaction to be more sensitive to pressure than that for the OH + butadiene reaction. Future studies will probe this effect in greater detail and for all isoprene−OH and butadiene−OH adducts.[67]

VI. Conclusions

The measured rate constants for the reaction of OH with 1,3-butadiene between 1 and 6 Torr and between 353 and 423 K are in good agreement with those obtained at higher pressures, suggesting that the rate constant for the OH + 1,3-butadiene reaction is at its high-pressure limit at pressures as low as 1 Torr and at temperatures as high as 423 K, in contrast to similar measurements for the OH + isoprene, methyl vinyl ketone, and methyl butenol reactions. The absence of a significant kinetic isotope effect for the OH + 1,3-butadiene-d_6 rate constant confirms that the primary mechanism for this reaction is OH addition even at the low pressure and high temperatures of these experiments.

The absence of a pressure dependence in the rate constant for the OH + 1,3-butadiene reaction is surprising given the fewer vibrational degrees of freedom available to distribute the excess energy associated with OH addition compared to the larger isoprene, methyl vinyl ketone, and methyl butenol reaction systems. One possible explanation for these results is that the hydroxyalkyl radicals produced from the OH + 1,3-butadiene react more quickly with O_2 to form hydroxyalkyl peroxy radicals than the corresponding radicals in the OH + isoprene reaction system, reducing the lifetime of these radicals. As a result, decomposition of the hydroxyalkyl radicals leading to the formation of reactants may not be able to compete with both stabilization and reaction with O_2 at higher temperatures, resulting in an absence of an observed pressure dependence for the OH + 1,3-butadiene reaction compared to that for the OH + isoprene reactions.

Another possible explanation for the lack of an observed pressure dependence for the OH + butadiene reaction compared to that for the OH + isoprene reaction at low pressures and temperatures above room temperature is that the intramolecular vibrational redistribution (IVR) associated with addition of OH to 1,3-butadiene is more efficient than the intramolecular transfer of energy associated with addition of OH to isoprene. Ab initio molecular dynamics calculations suggest that the mechanism of intramolecular transfer of energy in the OH + isoprene reaction is significantly different than that for the OH + butadiene reaction, involving the formation of stable five-membered rings that are responsible for energy transfer from the OH and CO stretch modes into the various CH bend and wag modes of the isoprene−OH adduct molecules. Further studies are needed to determine whether this difference in the mechanism of IVR between the OH + isoprene and the OH +1,3-butadiene reactions can account for the difference in the observed kinetics.

Acknowledgment. This work was supported by the National Science Foundation, Grant ATM-0612738 (P.S.S.), and the Petroleum Research Fund, Grant PRF-43489-G, administered by the American Chemical Society (S.S.I.). Authors S.S.I. and A.B.P. thank Scott Dietrick for his contributions to the IVR studies.

References and Notes

(1) United States Environmental Protection Agency. Locating and Estimating Air Emissions from Sources of 1,3-Butadiene; EPA-454/R-96-008; Office of Air Quality Planning and Standards: Research Triangle Park, NC, 1996.

(2) United States Environmental Protection Agency. Health Assessment of 1,3-Butadiene; EPA/600/P-98/001F; Office of Research and Development: Washington, DC, 2002.

(3) Acquavella, J. F. *Toxicology* **1996**, *113*, 148.

(4) Dollard, G. J.; Dore, C. J.; Jenkin, M. E. *Chem. Biol. Interact.* **2001**, *135*, 177.

(5) Anttinen-Klemetti, T.; Vaaranrinta, R.; Mutanen, P.; Peltonen, K. *Int. J. Hyg. Environ. Health* **2006**, *209*, 151.
(6) Eatough, D. J.; Hansen, L. D.; Lewis, E. A. *Environ. Technol.* **1990**, *11*, 1071.
(7) Pankow, J. F.; Luo, W.; Tavakoli, A. D.; Chen, C.; Isabelle, L. M. *Chem. Res. Toxicol.* **2004**, *17*, 805.
(8) Penn, A.; Snyder, C. A. *Circulation* **1996**, *93*, 552.
(9) Ye, Y.; Galbally, I. E.; Weeks, I. A.; Duffy, B. L.; Nelson, P. F. *Atmos. Environ.* **1998**, *32*, 2685.
(10) Thornton-Manning, J. R.; Dahl, A. R.; Bechtold, W. E.; Griffith, W. C.; Henderson, R. F. *Toxicology* **1997**, *123*, 125.
(11) Sorsa, M.; Peltonen, K.; Anderson, D.; Demopoulos, N. A.; Neumann, H. G.; OstermanGolkar, S. *Mutagenesis* **1996**, *11*, 9.
(12) Hurst, H. E. *Rev. Environ. Contam. Toxicol.* **2007**, *189*, 131.
(13) Cote, I. L.; Bayard, S. P. *Environ. Health Perspect.* **1990**, *86*, 149.
(14) Duffy, B. L.; Nelson, P. F. *Atmos. Environ.* **1997**, *31*, 3877.
(15) Duffy, B. L.; Nelson, P. F. *Atmos. Environ.* **1996**, *30*, 2759.
(16) Hughes, K.; Meek, M. E.; Walker, M. *Chem. Biol. Interact.* **2001**, *135*, 109.
(17) Liu, X. Y.; Jeffries, H. E.; Sexton, K. G. *Atmos. Environ.* **1999**, *33*, 3005.
(18) Notario, A.; Le Bras, G.; Mellouki, A. *Chem. Phys. Lett.* **1997**, *281*, 421.
(19) Tuazon, E. C.; Alvarado, A.; Aschmann, S. M.; Atkinson, R.; Arey, J. *Environ. Sci. Technol.* **1999**, *33*, 3586.
(20) Li, Z. J.; Nguyen, P.; de Leon, M. F.; Wang, J. H.; Han, K. L.; He, G. Z. *J. Phys. Chem. A* **2006**, *110*, 2698.
(21) Atkinson, R.; Arey, J. *Atmos. Environ.* **2003**, *37*, S197.
(22) Sprengnether, M.; Demerjian, K. L.; Donahue, N. M.; Anderson, J. G. *J. Geophys. Res.* **2002**, *107*, 4268.
(23) Baker, J.; Arey, J.; Atkinson, R. *Environ. Sci. Technol.* **2005**, *39*, 4091.
(24) Maldotti, A.; Chiorboli, C.; Bignozzi, C. A.; Bartocci, C.; Carassiti, V. *Int. J. Chem. Kinet.* **1980**, *12*, 905.
(25) Ohta, T. *Bull. Chem. Soc. Jpn.* **1984**, *57*, 960.
(26) Berndt, T.; Boge, O. *J. Phys. Chem. A* **2007**, *111*, 12099.
(27) Atkinson, R.; Perry, R. A.; Pitts, J. N. *J. Chem. Phys.* **1977**, *67*, 3170.
(28) Liu, A.; Mulac, W. A.; Jonah, C. D. *J. Phys. Chem.* **1988**, *92*, 131.
(29) Lloyd, A. C.; Darnall, K. R.; Winer, A. M.; Pitts, J. N. *J. Phys. Chem.* **1976**, *80*, 789.
(30) Chuong, B.; Stevens, P. S. *J. Phys. Chem. A* **2000**, *104*, 5230.
(31) McGivern, W. S.; Suh, I.; Clinkenbeard, A. D.; Zhang, R. Y.; North, S. W. *J. Phys. Chem. A* **2000**, *104*, 6609.
(32) Chuong, B.; Davis, M.; Edwards, M.; Stevens, P. S. *Int. J. Chem. Kinet.* **2002**, *34*, 300.
(33) Baasandorj, M.; Stevens, P. S. *J. Phys. Chem. A* **2007**, *111*, 640.
(34) Stevens, P.; L'Esperance, D.; Chuong, B.; Martin, G. *Int. J. Chem. Kinet.* **1999**, *31*, 637.
(35) Chuong, B.; Stevens, P. S. *J. Phys. Chem. A* **2003**, *107*, 2185.
(36) Davis, M. E.; Drake, W.; Vimal, D.; Stevens, P. S. *J. Photochem. Photobiol., A* **2005**, *176*, 162.
(37) Chuong, B.; Stevens, P.S. *J. Geophys. Res* **2002**, *107*, 4162.
(38) Atkinson, R.; Aschmann, S. M. *Int. J. Chem. Kinet.* **1984**, *16*, 1175.
(39) Greenwald, E. E.; North, S. W.; Georgievskii, Y.; Klippenstein, S. J. *J. Phys. Chem. A* **2007**, *111*, 5582.
(40) Vimal, D.; Stevens, P. S. *J. Phys. Chem. A* **2006**, *110*, 11509.
(41) Atkinson, R.; Pitts, J. N. *J. Chem. Phys.* **1975**, *63*, 3591.
(42) Vakhtin, A. B.; Murphy, J. E.; Leone, S. R. *J. Phys. Chem. A* **2003**, *107*, 10055.
(43) Pastrana, A. V.; Carr, R. W. *J. Phys. Chem.* **1975**, *79*, 765.
(44) Kuo, C. H.; Lee, Y. P. *J. Phys. Chem.* **1991**, *95*, 1253.
(45) Tuazon, E. C.; Atkinson, R. *Int. J. Chem. Kinet.* **1990**, *22*, 591.
(46) Orlando, J. J.; Tyndall, G. S.; Paulson, S. E. *Geophys. Res. Lett.* **1999**, *26*, 2191.
(47) Ochando-Pardo, M.; Nebot-Gil, I.; Gonzalez-Lafont, A.; Lluch, J. M. *ChemPhysChem.* **2005**, *6*, 1567.
(48) Stevens, P. S.; Seymour, E.; Li, Z. J. *J. Phys. Chem. A* **2000**, *104*, 5989.
(49) Singh, S.; Li, Z. *J. Phys. Chem. A* **2007**, *111*, 11843.
(50) Schlegel, H. B.; Millam, J. M.; Iyengar, S. S.; Voth, G. A.; Daniels, A. D.; Scuseria, G. E.; Frisch, M. J. *J. Chem. Phys.* **2001**, *114*, 9758.
(51) Iyengar, S. S.; Schlegel, H. B.; Millam, J. M.; Voth, G. A.; Scuseria, G. E.; Frisch, M. J. *J. Chem. Phys.* **2001**, *115*, 10291.
(52) Schlegel, H. B.; Iyengar, S. S.; Li, X.; Millam, J. M.; Voth, G. A.; Scuseria, G. E.; Frisch, M. J. *J. Chem. Phys.* **2002**, *117*, 8694.
(53) Iyengar, S. S.; Schlegel, H. B.; Voth, G. A.; Millam, J. M.; Scuseria, G. E.; Frisch, M. J. *Isr. J. Chem.* **2002**, *42*, 191.
(54) Iyengar, S. S.; Frisch, M. J. *J. Chem. Phys.* **2004**, *121*, 5061.
(55) Iyengar, S. S.; Day, T. J. F.; Voth, G. A. *Int. J. Mass. Spectrom.* **2005**, *241*, 197.
(56) Wang, I. S. Y.; Karplus, M. *J. Am. Chem. Soc.* **1973**, *95*, 8160.
(57) Leforestier, C. *J. Chem. Phys.* **1978**, *68*, 4406.
(58) Bolton, K.; Hase, W. L.; Peslherbe, G. H. *Modern Methods for Multidimensional Dynamics Computation in Chemistry*; World Scientific: Singapore, 1998.
(59) Payne, M. C.; Teter, M. P.; Allan, D. C.; Arias, T. A.; Joannopoulos, J. D. *Rev. Mod. Phys.* **1992**, *64*, 1045.
(60) Li, X.; Teige, V. E.; Iyengar, S. S. *J. Phys. Chem. A* **2007**, *111*, 4185.
(61) Iyengar, S. S. *J. Chem. Phys.* **2007**, *126*, 216101.
(62) Iyengar, S. S.; Peterson, M. K.; Day, T. J. F.; Burnham, C. J.; Teige, V. E.; Voth, G. A. *J. Chem. Phys.* **2005**, *123*, 84309.
(63) Iyengar, S. S. *J. Chem. Phys.* **2005**, *123*, 84310.
(64) Svozil, D.; Jungwirth, P. *J. Phys. Chem. A* **2006**, *110*, 9194.
(65) Sadhukhan, S.; Munoz, D.; Adamo, C.; Scuseria, G. E. *Chem. Phys. Lett.* **1999**, *306*, 83.
(66) Iyengar, S. S.; Li, X.; Sumner, I. *Adv. Quant. Chem.* **2008**, In press.
(67) Pacheco, A. B. ;Dietric, S. M.; Iyengar, S. S.; Stevens, P. S. Manuscript in preparation.
(68) Sumner, I.; Iyengar, S. S. *J. Phys. Chem. A* **2007**, *111*, 10313.
(69) Li, X.; Moore, D. T.; Iyengar, S. S. *J. Chem. Phys.* In Press.
(70) Frisch, M. J. Trucks, G. W.; Schlegel, H. B.; Scuseria, G. E.; Robb, M. A.; Cheeseman, J. R.; Montgomery, J. A., Jr.; Vreven, T.; Kudin, K. N.; Burant, J. C.; Millam, J. M.; Iyengar, S. S.; Tomasi, J.; Barone, V.; Mennucci, B.; Cossi, M.; Scalmani, G.; Rega, N.; Petersson, G. A.; Nakatsuji, H.; Hada, M.; Ehara, M.; Toyota, K.; Fukuda, R.; Hasegawa, J.; Ishida, M.; Nakajima, T.; Honda, Y.; Kitao, O.; Nakai, H.; Klene, M.; Li, X.; Knox, J. E.; Hratchian, H. P.; Cross, J. B.; Bakken, V.; Adamo, C.; Jaramillo, J.; Gomperts, R.; Stratmann, R. E.; Yazyev, O.; Austin, A. J.; Cammi, R.; Pomelli, C.; Ochterski, J. W.; Ayala, P. Y.; Morokuma, K.; Voth, G. A.; Salvador, P.; Dannenberg, J. J.; Zakrzewski, V. G.; Dapprich, S.; Daniels, A. D.; Strain, M. C.; Farkas, O.; Malick, D. K.; Rabuck, A. D.; Raghavachari, K.; Foresman, J. B.; Ortiz, J. V.; Cui, Q.; Baboul, A. G.; Clifford, S.; Cioslowski, J.; Stefanov, B. B.; Liu, G.; Liashenko, A.; Piskorz, P.; Komaromi, I.; Martin, R. L.; Fox, D. J.; Keith, T.; Al-Laham, M. A.; Peng, C. Y.; Nanayakkara, A.; Challacombe, M.; Gill, P. M. W.; Johnson, B.; Chen, W.; Wong, M. W.; Gonzalez, C.; Pople, J. A. *Gaussian 03*, revision B.01; Gaussian, Inc.: Wallingford, CT, 2003.
(71) Jensen, F. *Introduction to Computational Chemistry*, 2nd ed.; John Wiley and Sons: New York, 2006.
(72) Shin, J.-W.; Hammer, N. I.; Diken, E. G.; Johnson, M. A.; Walters, R. S.; Jaeger, T. D.; Duncan, M. A.; Christie, R. A.; Jordan, K. D. *Science* **2004**, *304*, 1137.
(73) Hammer, N. I.; Diken, E. G.; Roscioli, J. R.; Johnson, M. A.; Myshankin, E. M.; Jordan, K. D.; McCoy, A. B.; Huang, X.; Bowman, J. M.; Carter, S. *J. Chem. Phys.* **2005**, *122*, 244301.
(74) Diken, E. G.; Headrick, J. M.; Roscioli, J. R.; Bopp, J. C.; Johnson, M. A.; McCoy, A. B. *J. Phys. Chem. A* **2005**, *109*, 1487.
(75) Press, W. H.; Teukolsky, S. A.; Vetterling, W. T.; Flannery, B. P. *Numerical Recipes in C*, 2nd ed.; Cambridge University Press: New York, 1992.

JP8003882